

# Robust Spacecraft Low-Thrust Trajectory Design: A Chance-Constrained Covariance-Steering Approach

Meysam Babapour<sup>1</sup>, Ehsan Taheri<sup>1</sup>

**Abstract**—This paper proposes a systematic method for generating practical and robust low-thrust spacecraft trajectories. One contribution is to consider the change in mass of the spacecraft at two levels: a) the propulsive acceleration and b) the intensity of the stochastic disturbances. A *covariance variable* formulation is considered, which is computationally more efficient than the factorized covariance implementation. The proposed approach is applied to two- (i.e., planar) and three-dimensional heliocentric phases of spacecraft flight from Earth to Mars under the restricted two-body dynamics. The results highlight the importance of keeping track of mass change to generate more realistic, robust solutions for interplanetary space missions to avoid underestimation of mission risks.

## I. INTRODUCTION

Optimal control principles (OCPs) are used extensively for spacecraft trajectory design [1], [2], [3]. The study of OCPs under uncertainty has a long history. The early developments were grounded in problems solved through dynamic programming (DP), a rigorous framework for sequential decision-making, but severely limited in its applicability to realistic high-dimensional systems [4], [5]. To address computational barriers, approximate methods such as differential dynamic programming (DDP) were developed, which iteratively refine control laws by local quadratic approximations of the so-called value function [6]. These methods reduce computational complexity, but faces difficulties when nonlinear dynamics, nonconvex constraints, or non-Gaussian uncertainties have to be considered [7].

For unconstrained linear stochastic systems, the state mean and covariance evolve independently. The mean trajectory is governed by the feedforward control inputs, while the covariance dynamics is shaped by the choice of state feedback gains. This decoupling property underlies the observation that solutions to covariance-steering problems with quadratic costs are closely related to Linear Quadratic Regulator (LQR)-based formulations, where feedback laws naturally regulate state dispersion [8], [9], [10].

The independence between mean and covariance no longer holds once constraints are present, and thus mean and covariance dynamics become tightly coupled. As a result, standard LQR methods are not sufficient to address the complexity of practical problems. Alternative approaches have sought to integrate LQR with stochastic optimization. One such strategy consists of designing a feedback gain *a priori* using LQR and then optimizing only the feedforward control component within a stochastic framework [11]. A

more flexible formulation treats the feedback gain as an optimization variable, enabling joint design of feedforward and feedback terms to better handle nonlinearities, nonconvex and probabilistic constraints, and covariance propagation. The resulting non-convex problems are typically solved using sequential convex programming (SCP).

The *factorized covariance* formulation method is proposed in [12], [13], [14] that applies an SCP approach to solve covariance-steering problems. However, factorized covariance formulations are computationally expensive, as each subproblem involves a linear matrix inequality (LMI) whose dimensions grow quadratically with the number of nodes,  $N$ , leading to a complexity of  $\mathcal{O}(N^2 n_x n_u)$  (with  $n_x$  and  $n_u$  denoting the dimensions of state and control vectors, respectively). An alternative *covariance variable* SCP-based formulation was introduced in [15]. Nevertheless, the proof of lossless convexification underpinning this method was later shown to be incorrect [16]. A subsequent modification by [17] (based on the original work [18]) is also proposed to restore the validity of the formulation under the assumption that a set of tight tolerances are satisfied. Covariance-steering formulations are used for a variety of applications, from powered descent guidance [19] to spacecraft rendezvous and docking maneuvers [20].

**Contributions:** 1) We investigate the application of the *covariance variable* SCP-based formulation for solving fuel-optimal low-thrust Earth-to-Mars problems, which explicitly models spacecraft mass dynamics. This formulation a) allows for thrust to be considered as the control input and b) models a mass-varying stochastic force intensity. In previous low-thrust trajectory studies, the mass is not considered as a state. The mass time rate of change is an essential component of the acceleration term that appears in the equations of motion. The advantage of this model is that we can consider realistic engine parameters (such as thrust magnitude and specific impulse) and enforce constraints directly on the maximum thrust that is to be produced by the propulsion system.

2) We also review the steps for implementing a *covariance variable* formulation, mirroring the steps outlined in Ref. [17], which is computationally more efficient than the *factorized covariance* implementation. However, we provide particular modifications needed for considering the variation in mass. A detailed analysis of the results is also presented. The paper is structured with Sec. II introducing the general formulation of the stochastic OCP. Section III describes the detailed convexification procedure and the iterative algorithm. The proposed approach is then assessed in Section IV through numerical simulations on a more realistic scenario.

<sup>1</sup>Meysam Babapour and Ehsan Taheri are with the Department of Aerospace Engineering, Auburn University, Auburn, AL USA, {mzb0218, ezt0028}@auburn.edu.

Finally, Section V presents concluding remarks with potential directions for future research.

The notation used in this paper is standard. In particular,  $\mathbb{E}[\cdot]$  denotes the expectation operator,  $\mathbb{P}(\cdot)$  denotes the probability measure, and  $\mathbb{S}_+^n$  is a set of all positive definite matrices of dimension  $n$ . Also,  $x_t = x(t)$  and  $u_t = u(t)$ .  $\mathbb{R}_+$  denotes the set of positive real numbers.  $I_n$  denotes an  $n$ -dimensional identity matrix.

## II. CHANCE-CONSTRAINED STOCHASTIC OPTIMAL CONTROL

### A. Continuous-Time Formulation

We consider a continuous-time nonlinear stochastic dynamical system governed by the stochastic differential equation (SDE), which can be written as,

$$dx_t = \mathbf{f}(x_t, u_t, t) dt + \mathbf{g}(x_t, u_t) dw_t, \quad t \in [t_0, t_f], \quad (1)$$

where  $x_t \in \mathbb{R}^{n_x}$  denotes the system state,  $u_t \in \mathbb{R}^{n_u}$  is the control input, and  $\mathbf{f} : \mathbb{R}^{n_x} \times \mathbb{R}^{n_u} \times \mathbb{R} \rightarrow \mathbb{R}^{n_x}$  represents the drift dynamics. The diffusion term  $\mathbf{g} : \mathbb{R}^{n_x} \times \mathbb{R}^{n_u} \rightarrow \mathbb{R}^{n_x \times n_w}$  maps the disturbance to the state space, where  $w_t \in \mathbb{R}^{n_w}$  is a standard Wiener process with independent increments satisfying  $\mathbb{E}[dw_t] = \mathbf{0}_{n_w}$  and  $\mathbb{E}[dw_t dw_t^\top] = I_{n_w} dt$ .

Our goal is to steer the trajectory of the system (1) from a normally distributed initial condition  $x_{t_0}$  to a desired/specified final distribution  $x_{t_f}$

$$x_{t_0} \sim \mathcal{N}(\bar{x}_i, P_i), \quad x_{t_f} \sim \mathcal{N}(\bar{x}_f, P_f), \quad (2)$$

where  $\bar{x}_i, \bar{x}_f \in \mathbb{R}^{n_x}$  are the initial and desired terminal mean states, and  $P_i, P_f \in \mathbb{S}_+^{n_x}$  are the corresponding covariance matrices. To achieve this, we seek a control policy  $u_t = \pi(x_t, t)$  that simultaneously regulates both the mean state trajectory and the covariance evolution. We employ a piecewise constant affine control of the form

$$u_t = v_t + K_t(x_t - \bar{x}_t), \quad t \in [t_0, t_f], \quad (3)$$

where  $v_t \in \mathbb{R}^{n_u}$  denotes the nominal control sequence,  $K_t \in \mathbb{R}^{n_u \times n_x}$  is the feedback gain matrix.

Throughout the time horizon, the state and control trajectories must satisfy various operational and safety requirements. Since the state distribution and consequently the control input, as a state-feedback law, are unbounded under Gaussian assumption, these conditions have to be imposed probabilistically as chance constraints, which can be written as,

$$\mathbb{P}(\mathbf{h}(x_t, u_t) \leq 0) \geq \beta, \quad t \in [t_0, t_f], \quad (4)$$

where  $0 < \beta < 1$  denotes the desired confidence level.

In practice, the control authority is limited,  $\|u_t\| \leq u_{\max}$ . This constraint is enforced by specializing the general chance constraint (4) to the control input as,

$$\mathbb{P}(\|u_t\| \leq u_{\max}) \geq \beta_u, \quad t \in [t_0, t_f], \quad (5)$$

where  $u_{\max} > 0$  is the maximum available control effort and  $\beta_u$  is its associated confidence level.

While satisfying all constraints, the control objective is also to minimize the control effort. A Lagrange form of the cost functional is written as,

$$J = \int_{t_0}^{t_f} \|u_t\| dt. \quad (6)$$

The performance index (6), however, is not directly tractable, as it involves integration of a stochastic process. To obtain a numerically tractable objective, we reformulate the cost using the  $p$ -quantile of the stochastic control norm, which accounts for both the mean control effort and its variability, leading to

$$J_1 = Q\left(\int_{t_0}^{t_f} \|u_t\| dt; p\right), \quad 0 < p < 1, \quad (7)$$

where  $Q(\cdot; p)$  denotes the quantile operator. The continuous-time nonlinear chance-constrained stochastic optimal control problem can be stated as Problem 1.

Problem 1 (Chance-Constrained SOC Optimization)

$$\min_{u_t} J_1 = Q\left(\int_{t_0}^{t_f} \|u_t\| dt; p\right) \quad (8a)$$

$$\text{s.t. } dx_t = \mathbf{f}(x_t, u_t, t) dt + \mathbf{g}(x_t, u_t) dw_t, \quad (8b)$$

$$x_{t_0} \sim \mathcal{N}(\bar{x}_i, P_i), \quad (8c)$$

$$\mathbb{P}(\|u_t\| \leq u_{\max}) \geq \beta_u, \quad t \in [t_0, t_f], \quad (8d)$$

$$x_{t_f} \sim \mathcal{N}(\bar{x}_f, P_f), \quad (8e)$$

$$u_t = v_t + K_t(x_t - \bar{x}_t), \quad t \in [t_0, t_f]. \quad (8f)$$

### B. Discrete-Time Deterministic Formulation

To formulate a tractable optimization problem, the nonlinear stochastic dynamics (1) are approximated by a linear continuous-time, time-varying stochastic system, which is valid under the assumption of small deviations. Linearization around a reference trajectory  $(\hat{x}_t, \hat{u}_t)$  gives

$$dx_t = (A(t)x_t + B(t)u_t + c(t)) dt + G(t) dw_t \quad (9)$$

where  $G(t) = \mathbf{g}(\hat{x}_t, \hat{u}_t)$  and the other matrices are

$$A(t) = \frac{\partial \mathbf{f}}{\partial x}\Big|_{(\hat{x}_t, \hat{u}_t)}, \quad B(t) = \frac{\partial \mathbf{f}}{\partial u}\Big|_{(\hat{x}_t, \hat{u}_t)}, \quad (10)$$

$$c(t) = \mathbf{f}(\hat{x}_t, \hat{u}_t, t) - A(t)\hat{x}_t - B(t)\hat{u}_t. \quad (11)$$

With the zero-order hold assumption on the control input, the system is then discretized over the time horizon  $[t_0, t_f]$ , which is partitioned into  $N$  uniform segments. The resulting discrete-time, time-varying linear stochastic dynamics are

$$x_{k+1} = A_k x_k + B_k u_k + c_k + G_k w_k, \quad (12)$$

where  $k = 0, 1, \dots, N-1$  and the system matrices are obtained from the continuous-time dynamics using the state transition matrix,  $\Phi(t, \tau)$ , associated with  $A(t)$ , as follows

$$A_k = \Phi(t_{k+1}, t_k), \quad (13)$$

$$B_k = \int_{t_k}^{t_{k+1}} \Phi(t_{k+1}, \tau) B(\tau) d\tau, \quad (14)$$

$$\mathbf{c}_k = \int_{t_k}^{t_{k+1}} \Phi(t_{k+1}, \tau) \mathbf{c}(\tau) d\tau, \quad (15)$$

$$Q_k = \int_{t_k}^{t_{k+1}} \Phi(t_{k+1}, \tau) G(\tau) G(\tau)^\top \Phi(t_{k+1}, \tau)^\top d\tau, \quad (16)$$

where  $\Phi(t, \tau)$  is the solution to the matrix ordinary differential equation

$$\frac{d}{dt} \Phi(t, \tau) = A(t) \Phi(t, \tau), \quad \Phi(\tau, \tau) = \mathbf{I}_{n_x}, \quad (17)$$

and  $\mathbf{w}_k \sim \mathcal{N}(\mathbf{0}, \mathbf{I}_{n_w})$  denotes a sequence of independent and identically distributed (i.i.d.) Gaussian disturbances. The matrix  $G_k$  is chosen such that  $G_k G_k^\top = Q_k$ . The corresponding mean and covariance propagation dynamics of (12) are

$$\bar{\mathbf{x}}_{k+1} = A_k \bar{\mathbf{x}}_k + B_k \mathbf{v}_k + \mathbf{c}_k, \quad (18)$$

$$P_{k+1} = (A_k + B_k K_k) P_k (A_k + B_k K_k)^\top + Q_k, \quad (19)$$

with the corresponding initial and final conditions from (2),

$$\bar{\mathbf{x}}_0 = \bar{\mathbf{x}}_i, \quad P_0 = P_i, \quad \bar{\mathbf{x}}_N = \bar{\mathbf{x}}_f, \quad P_N = P_f. \quad (20)$$

The probabilistic control constraint (5) can be reformulated as a conservative deterministic constraint by applying the triangle inequality to the affine control policy as,

$$\|\mathbf{v}_k\| + \sqrt{Q_{\chi_{n_u}^2}(\beta_u)} \sqrt{\lambda_{\max}(K_k P_k K_k^\top)} \leq u_{\max}, \quad (21)$$

where  $Q_{\chi_{n_u}^2}(\beta_u)$  is  $\beta_u$ -quantile of the chi-squared distribution with  $n_u$  degrees of freedom,  $\lambda_{\max}(\cdot)$  denotes the largest eigenvalue, and  $K_k P_k K_k^\top$  is the control covariance matrix.

Similarly, the objective function (7) can be written in a discrete-time deterministic form of

$$J_2 = \sum_{k=0}^{N-1} \left( \|\mathbf{v}_k\| + \sqrt{Q_{\chi_{n_u}^2}(p)} \sqrt{\lambda_{\max}(K_k P_k K_k^\top)} \right). \quad (22)$$

Problem 2 (Discrete-Time Chance-Constrained Deterministic Covariance-Steering Optimization).

Let  $\mathbf{z}_2 = \{\bar{\mathbf{x}}, \mathbf{v}_k, P_k, K_k\}$ , the problem is

$$\min_{\mathbf{z}_2} J_2, \quad (23a)$$

$$\text{s.t. } \bar{\mathbf{x}}_{k+1} = A_k \bar{\mathbf{x}}_k + B_k \mathbf{v}_k + \mathbf{c}_k, \quad (23b)$$

$$P_{k+1} = (A_k + B_k K_k) P_k (A_k + B_k K_k)^\top + Q_k, \quad (23c)$$

$$\|\mathbf{v}_k\| + \sqrt{Q_{\chi_{n_u}^2}(\beta_u)} \sqrt{\lambda_{\max}(K_k P_k K_k^\top)} \leq u_{\max}, \quad (23d)$$

$$\bar{\mathbf{x}}_0 = \bar{\mathbf{x}}_i, \quad P_0 = P_i, \quad (23e)$$

$$\bar{\mathbf{x}}_N = \bar{\mathbf{x}}_f, \quad P_N = P_f, \quad (23f)$$

$$\mathbf{u}_k = \mathbf{v}_k + K_k (\mathbf{x}_k - \bar{\mathbf{x}}_k). \quad (23g)$$

### III. SEQUENTIAL CONVEX PROGRAMMING

We now present an SCP framework to compute a solution to Problem 2 through linearization and convexification.

#### A. Covariance Propagation

The covariance propagation dynamics (19) is bilinear in  $K_k$  and  $P_k$ . To convexify it, two auxiliary variables  $U_k = K_k P_k \in \mathbb{R}^{n_u \times n_x}$  and  $Y_k = K_k P_k K_k^\top \in \mathbb{S}_+^{n_u}$  are introduced [18]. Substituting these definitions into (19) yields the affine recursion as,

$$\begin{aligned} P_{k+1} = & A_k P_k A_k^\top + A_k U_k^\top B_k^\top \\ & + B_k U_k A_k^\top + B_k Y_k B_k^\top + Q_k. \end{aligned} \quad (24)$$

To ensure consistency between  $P_k$ ,  $U_k$ , and  $Y_k$ , the Schur-complement LMI constraint is imposed

$$\begin{bmatrix} P_k & U_k^\top \\ U_k & Y_k \end{bmatrix} \succeq 0. \quad (25)$$

#### B. Formulating Chance-Constraint Control

The deterministic equation of the probabilistic control constraint (21) is nonconvex due to square root of the spectral term  $\sqrt{\lambda_{\max}(Y_k)}$ . To convexify, we first introduce another auxiliary variable  $\tau_k \in \mathbb{R}_+$  as an upper bound of the maximum standard deviation of the control covariance

$$\lambda_{\max}(Y_k) \leq \tau_k^2, \quad (26)$$

and then linearize the quadratic term around a reference value of  $\hat{\tau}_k$ ,

$$\lambda_{\max}(Y_k) - \hat{\tau}_k^2 - 2\hat{\tau}_k(\tau_k - \hat{\tau}_k) \leq \zeta_k, \quad (27)$$

where  $\zeta_k \in \mathbb{R}_+$  is an additional slack variable to allow for small discrepancies due to linearization. The resulting convex second-order cone inequality constraint becomes

$$\|\mathbf{v}_k\| + \sqrt{Q_{\chi_{n_u}^2}(\beta_u)} \tau_k \leq u_{\max}. \quad (28)$$

#### C. Objective Function

In addition to replacing  $\lambda_{\max}(Y_k)$  with its upper bound  $\tau_k$  in (22), lossless convexification requires that the gradient with respect to  $Y_k$  be strictly positive [21],  $\frac{\partial J}{\partial Y_k} > 0$ . This requirement is not satisfied in the current formulation. To guarantee convexity, we augment the cost with a small regularization term involving the trace of  $Y_k$  [17] as,

$$J_3 = \sum_{k=0}^{N-1} \left( \|\mathbf{v}_k\| + \sqrt{Q_{\chi_{n_u}^2}(p)} \tau_k + \varepsilon_Y \text{tr}(Y_k) \right). \quad (29)$$

Furthermore, the slack variable  $\zeta_k$  introduced in (27) must be penalized to minimize the linearization error,

$$J_{\text{pen}} = \sum_{k=0}^{N-1} \left( \zeta_k + \frac{w}{2} \zeta_k^2 + \sqrt{w} \|\zeta\|_1 \right), \quad (30)$$

where  $w$  is a penalty coefficient.

Problem 3 (Convex SDP Covariance-Steering Problem). Let  $\mathbf{z}_3 = \{\bar{\mathbf{x}}, \mathbf{v}_k, P_k, U_k, Y_k, \tau_k, \zeta_k\}$ , the convex SDP problem, which is solved at each SCP iteration, is written as,

$$\min_{\mathbf{z}_3} J_{\text{aug}} = J_3 + J_{\text{pen}}, \quad (31a)$$

$$\text{s.t. } \bar{\mathbf{x}}_{k+1} = A_k \bar{\mathbf{x}}_k + B_k \mathbf{v}_k + \mathbf{c}_k, \quad (31b)$$

$$\begin{aligned} P_{k+1} &= A_k P_k A_k^\top + A_k U_k^\top B_k^\top \\ &\quad + B_k U_k A_k^\top + B_k Y_k B_k^\top + Q_k, \end{aligned} \quad (31c)$$

$$\begin{bmatrix} P_k & U_k^\top \\ U_k & Y_k \end{bmatrix} \succeq 0, \quad (31d)$$

$$\|\mathbf{v}_k\| + \sqrt{Q_{\chi_{n_u}^2}(\beta_u)} \tau_k \leq u_{\max}, \quad (31e)$$

$$\lambda_{\max}(Y_k) - \hat{\tau}_k^2 - 2\hat{\tau}_k(\tau_k - \hat{\tau}_k) \leq \zeta_k, \quad (31f)$$

$$\bar{\mathbf{x}}_0 = \bar{\mathbf{x}}_i, P_0 = P_i, \bar{\mathbf{x}}_N = \bar{\mathbf{x}}_f, P_N = P_f. \quad (31g)$$

This convex reformulation removes bilinearities while preserving the structural coupling between covariance and feedback terms. Regularization of  $Y_k$  in the cost discourages artificial inflation of these terms and ensures conservative yet effective control of uncertainty. The procedure for solving Problem 3 is summarized in Algorithm 1 below.

Algorithm 1 (Sequential Convex Programming).

- 1) Initialization: choose a nominal feasible trajectory  $\{\bar{\mathbf{x}}_k, \mathbf{v}_k, \hat{\tau}_k\}$  and select penalty weights  $\varepsilon_Y, w > 0$ .
- 2) Convexification: Linearize and discretize to obtain  $\{A_k, B_k, \mathbf{c}_k, Q_k\}$ .
- 3) Solve Convex SDP: solve problem 3 to obtain  $\mathbf{z} = \{\bar{\mathbf{x}}_k^*, \mathbf{v}_k^*, P_k^*, U_k^*, Y_k^*, \tau_k^*, \zeta_k^*\}$ .
- 4) Reference Update: set  $\mathbf{z}_k \leftarrow \mathbf{z}_k^*$ .
- 5) Iterate until the solution converges.

#### IV. NUMERICAL SIMULATIONS

##### A. Planar low-thrust Earth-to-Mars problem

We consider a planar low-thrust Earth-to-Mars rendezvous problem with zero hyperbolic excess velocities [22]. The spacecraft dynamics are modeled in a Sun-centered Cartesian inertial frame restricted to the ecliptic plane written as,

$$\mathbf{f}(\mathbf{x}_t, \mathbf{u}_t, t) = \begin{bmatrix} \mathbf{v}_t \\ -\mu \frac{\mathbf{r}_t}{\|\mathbf{r}_t\|^3} + \frac{\mathbf{u}_t}{m_t} \\ -\frac{\|\mathbf{u}_t\|}{I_{\text{sp}} g_0} \end{bmatrix}, \quad (32)$$

where  $\mathbf{x}_t = [\mathbf{r}_t^\top, \mathbf{v}_t^\top, m_t]^\top \in \mathbb{R}^5$  is the state vector, with  $\mathbf{r}_t \in \mathbb{R}^2$  the position,  $\mathbf{v}_t \in \mathbb{R}^2$  the velocity, and  $m_t \in \mathbb{R}$  the spacecraft mass. The control input,  $\mathbf{u}_t \in \mathbb{R}^2$ , represents the thrust vector. The parameter  $\mu$  denotes the Sun's gravitational parameter, and  $I_{\text{sp}}$  and  $g_0$  are the specific impulse and Sea-level gravity values, respectively. We consider the inclusion of mass because its change significantly influences both the optimal trajectory and the stochastic behavior of the system, unlike many simplified models [13], [15]. In addition, we can consider the thrust magnitude as the control input, which is more practical as opposed to considering maximum

acceleration [23]. The corresponding SDEs become

$$d \begin{bmatrix} \mathbf{r}_t \\ \mathbf{v}_t \\ m_t \end{bmatrix} = \mathbf{f}(\mathbf{x}_t, \mathbf{u}_t, t) dt + \begin{bmatrix} \mathbf{0}_{2 \times 2} \\ \frac{\gamma}{m_t} I_2 \\ \mathbf{0}_{1 \times 2} \end{bmatrix} d\mathbf{w}_t, \quad (33)$$

where  $d\mathbf{w}_t \in \mathbb{R}^2$  is a two-dimensional Wiener process with independent increments and  $\gamma$  is the force disturbance intensity. The diffusion term scales  $\gamma$  by the inverse of the instantaneous spacecraft mass. Thus, as  $m_t$  decreases, the same level of force uncertainty induces a larger stochastic acceleration disturbance. The continuous-time dynamics are linearized according to Eqs. (10-11) and subsequently discretized by Eqs. (13-17) over  $N = 40$  time intervals. The initial reference trajectory, required for linearization, is obtained by solving a minimum-fuel deterministic version of the problem using the CasADi solver [24] following the work in [23]. The boundary conditions, along with the relevant physical and mission parameters, are summarized in Table I. Although the chosen disturbance intensity (i.e.,  $\gamma/m(t_0)$ ) is

TABLE I: Parameters for the planar Earth-to-Mars problem.

Parameter	Value	Unit
$r_i$	$[-140699693; -51614428]$	km
$v_i$	$[9.774596; -28.07828]$	km/s
$r_f$	$[-172682023; 176959469]$	km
$v_f$	$[-16.427384; -14.860506]$	km/s
$m_i$	5000	kg
$\sigma_{r_i}$	10	km
$\sigma_{v_i}$	0.1	km/s
$\sigma_{r_f}$	$3.16 \times 10^5$	km
$\sigma_{v_f}$	0.1	km/s
$\mu$	$1.3271 \times 10^{11}$	$\text{km}^3/\text{s}^2$
$I_{\text{sp}}$	3000	s
$g_0$	9.80665	$\text{m/s}^2$
$u_{\max}$	5	N
$\gamma$	$9 \times 10^{-5}$	$\text{kg} \cdot \text{km/s}^{3/2}$
$t_f$	348.795	day
$d$	100	—
$p, \beta_u$	0.95	—

comparable to the magnitude reported in the literature [13], [15], the effective disturbance level exceeds those values by the end of the maneuver due to the decreasing spacecraft mass. Note that  $m(t_0)$  is assumed to be deterministic at departure and a large terminal mass covariance is permitted, reflecting the fact that the control objective does not involve regulating the final mass uncertainty.

To avoid numerical conditioning issues during optimization, all problem data are properly scaled. In particular, the covariance dynamics and related constraints are scaled following the approach proposed in [17], with a scaling factor of  $d$ . The SCP algorithm terminates when the relative difference between consecutive state trajectories satisfies

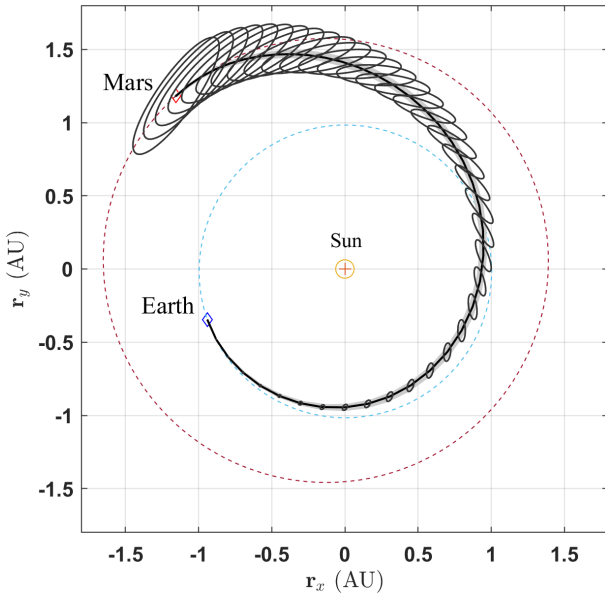
$$\frac{\|\mathbf{x}^{(i)} - \mathbf{x}^{(i-1)}\|}{\|\mathbf{x}^{(i-1)}\|} \leq \varepsilon_x, \quad \varepsilon_x = 5 \times 10^{-4},$$

where  $(i)$  denotes the SCP iteration and the linearization slack variable satisfies  $\zeta \leq \varepsilon_\zeta = 10^{-6}$ . Penalty coefficient

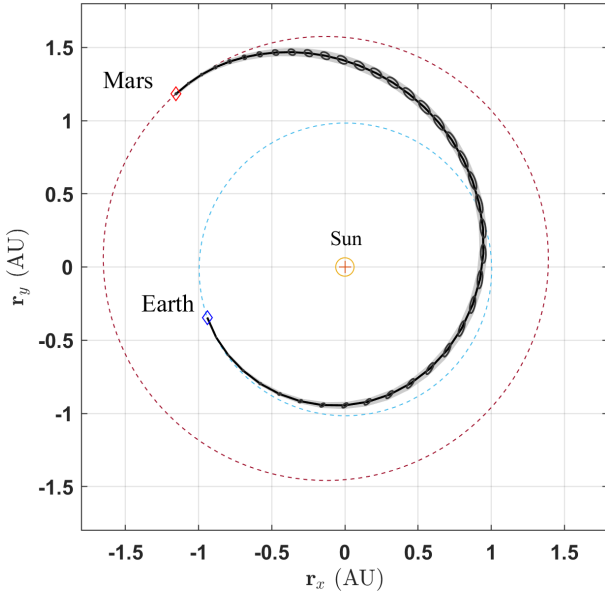
$w$  is updated at each iteration,  $i$ , as,

$$w = \min \left( 10^{(i+3)}, 10^{12} \right).$$

Problem 3 is solved and the convergence is achieved in 12 iterations (6.01 s) on an Intel® Core™ i7-13620H @ 2.40 GHz laptop computer. Figure 1 depicts the evolution of the position covariance along with the mean trajectory. In the open-loop case, the covariance grows rapidly over time, whereas in the closed-loop case, the 95%-confidence ellipses remain bounded due to the action of the feedback controller. A Monte Carlo simulation (with 1000 samples) was used



(a) Open-loop position covariance.



(b) Closed-loop position covariance.

Fig. 1: Position covariances.

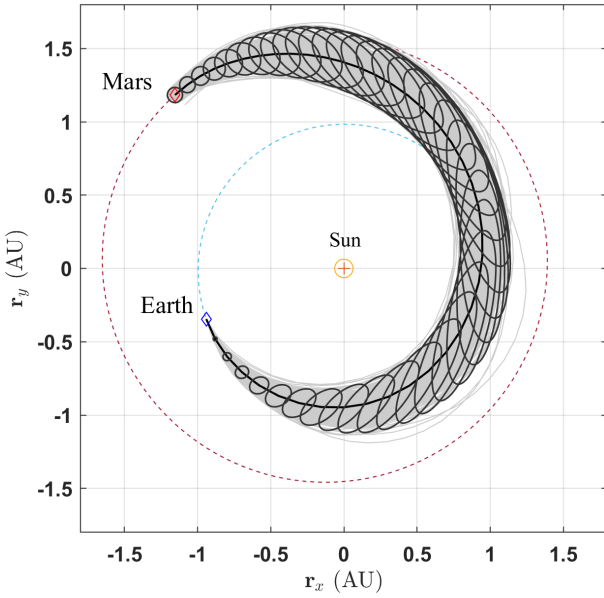
to validate the optimized trajectory. Figure 2 compares the resulting dispersion with the nominal solution in which both

position and velocity covariance ellipses in Figs. 2a and 2b are enlarged tenfold for improved visual interpretation. The close alignment of position and velocity samples within their predicted uncertainty ellipses validates the precision of the covariance propagation framework.

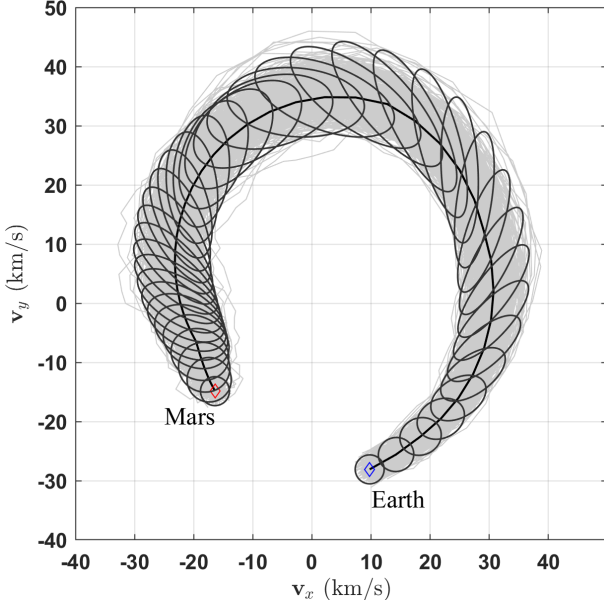
Figure 3 depicts the control profiles and its components. Figure 3a shows the closed-loop nominal control ( $v$ ) and Monte Carlo simulation (1000 samples) profiles. While the feedforward control consists of three main thrust arcs (similar to the deterministic solution for the same problem [22]), the magnitude of the thrust shows noticeable deviations from a clean bang-bang profile. This is a direct consequence of trading off robustness for pure fuel optimality, which requires the mean thrust to create some margins for the feedback term to control the covariances, which has occurred mainly during the last two thrust arcs. Figure 3b shows the components of the nominal control with feedback gain uncertainty ellipses.

Figure 4 shows the time histories of the mass and its standard deviation along the trajectory. The mass decreases by approximately 25% over the course of the mission, reaching a final value of approximately  $m_f = 3775$  kg upon arrival at Mars. The velocity standard deviation, shown in Figure 5, exhibits a significant growth over the mission horizon when the mass uncertainty is included, with peak standard deviations increasing by up to 16.79%. A similar trend is expected in the evolution of the position uncertainty and, as Figure 6 shows the trace of the position covariances, mass inclusion results in 33.27% higher dispersion at mid-course phase. These differences underscore the indirect amplification mechanism by which uncertainty in mass, originating from stochastic control input norms, propagates through the dynamics and inflates the velocity variance due to the  $1/m$  coupling in the translational acceleration equation. Neglecting this effect leads to an underestimation of the control authority required to robustly satisfy the terminal state covariance constraints, especially in long-duration, low-thrust missions.

We highlight that the effect of explicitly modeling mass dynamics, as a stochastic decision variable, was rigorously evaluated by comparing two formulations of the chance-constraint covariance-steering problem. In the first scenario, the mass equation was incorporated as a fifth state, and its uncertainty was propagated through the full closed-loop covariance dynamics. In the second scenario, mass evolution was considered deterministic and excluded from the set of decision variables, effectively assuming that the thrust-to-acceleration mapping remained constant throughout the mission. Despite producing comparable nominal trajectories, the results reveal notable discrepancies in the control effort and state uncertainty, particularly during the thrusting phases. Figure 7 compares the closed-loop feedforward control profiles for the two scenarios. The results show that including mass uncertainty leads to noticeably higher thrust magnitudes during the main thrust arcs, with a peak increase of approximately 6% relative to the case without mass modeling.



(a) Closed-loop position covariances.



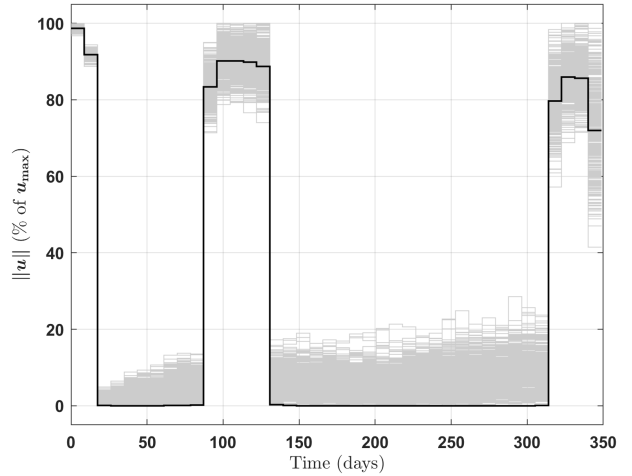
(b) Closed-loop velocity covariances.

Fig. 2: Position covariances (scaled 10x).

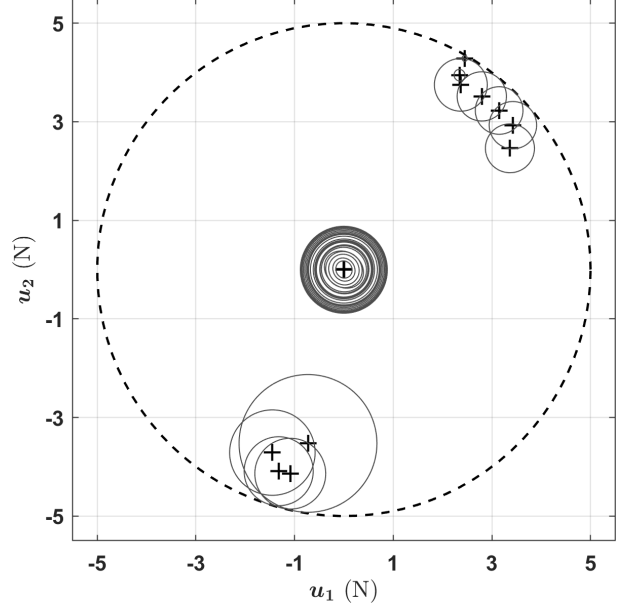
### B. Three-dimensional (3D) Earth-to-Mars problem

This case study presents a more realistic low-thrust Earth-to-Mars rendezvous to demonstrate the full capability of the proposed covariance steering framework.

The spacecraft dynamics are modeled in a Sun-centered Cartesian inertial frame, with the full state vector defined as  $\mathbf{x}_t = [\mathbf{r}_t^\top, \mathbf{v}_t^\top, m_t]^\top \in \mathbb{R}^7$ , where  $\mathbf{r}_t = [r_x, r_y, r_z]^\top \in \mathbb{R}^3$ ,  $\mathbf{v}_t = [v_x, v_y, v_z]^\top \in \mathbb{R}^3$  are the position and velocity vectors, respectively, and  $m_t \in \mathbb{R}_+$  is the spacecraft mass.



(a) Magnitude of the Monte Carlo control samples (gray) and closed-loop nominal control (black).



(b) Control with feedback gain uncertainty ellipses.

Fig. 3: Control mean and covariance evolution.

The dynamics are given by

$$\mathbf{f}(\mathbf{x}_t, \mathbf{u}_t, t) = \begin{bmatrix} \mathbf{v}_t \\ -\mu \frac{\mathbf{r}_t}{\|\mathbf{r}_t\|^3} + \frac{\mathbf{u}_t}{m_t} \\ -\frac{\|\mathbf{u}_t\|}{I_{sp}g_0} \end{bmatrix}, \quad (34)$$

where  $\mathbf{u}_t \in \mathbb{R}^3$  is the thrust vector,  $\mu$  is the Sun's gravitational parameter, and  $I_{sp}$  and  $g_0$  are the specific impulse and standard gravity, respectively. The mass dynamics are explicitly included to capture the critical coupling between fuel consumption and translational acceleration.

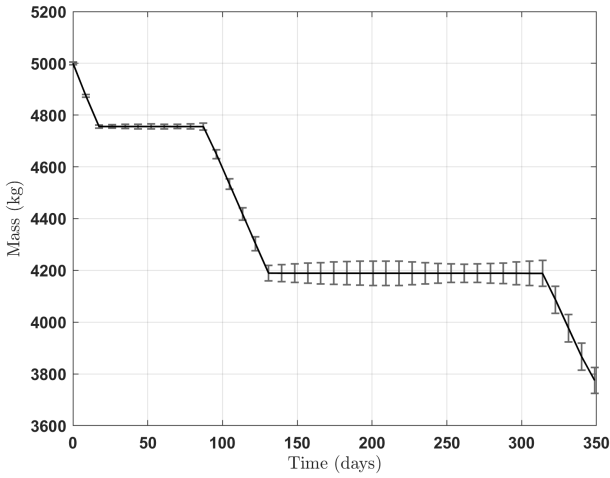


Fig. 4: Mass and its standard deviation vs. time.

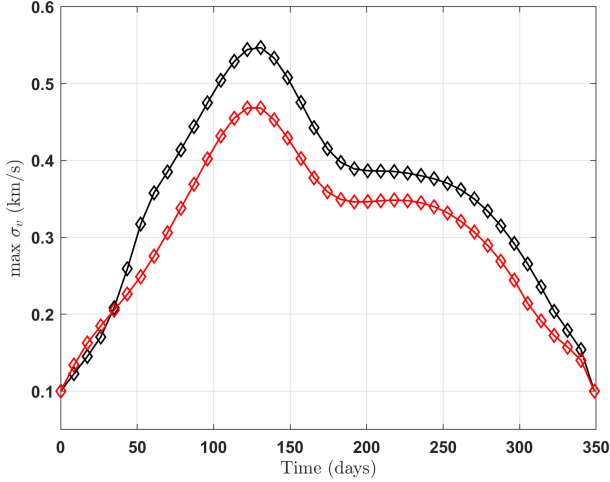


Fig. 5: Velocity standard deviation along first principle component with (black) and without (red) mass uncertainty.

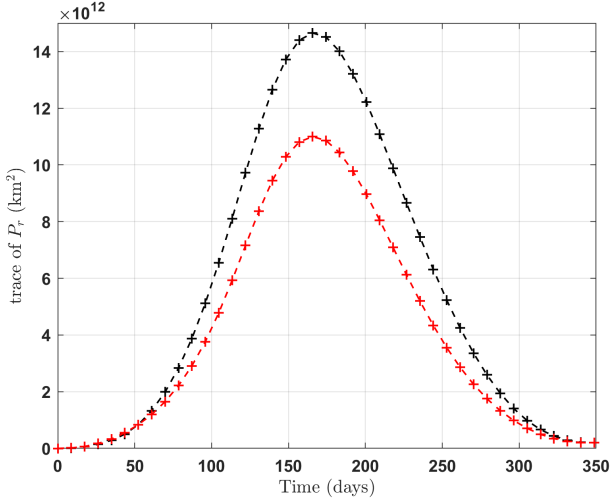


Fig. 6: Trace of the position covariances with (black) and without (red) the inclusion of mass uncertainty.

The corresponding stochastic differential equation is

$$d \begin{bmatrix} \mathbf{r}_t \\ \mathbf{v}_t \\ m_t \end{bmatrix} = \mathbf{f}(\mathbf{x}_t, \mathbf{u}_t, t) dt + \begin{bmatrix} \mathbf{0}_{3 \times 3} \\ \gamma I_3 \\ 0 \end{bmatrix} d\mathbf{w}_t, \quad (35)$$

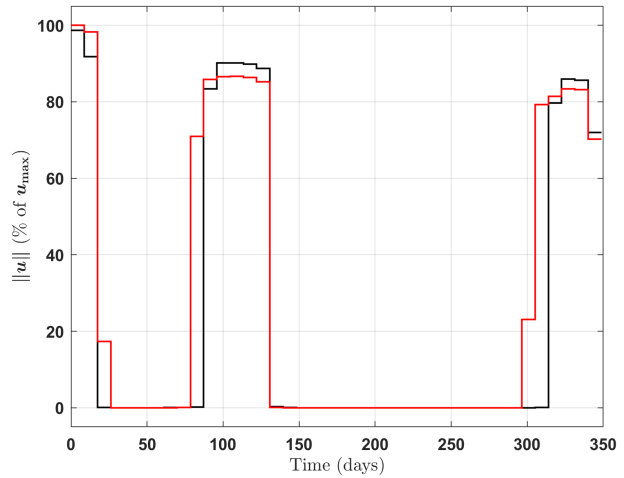


Fig. 7: Control w/ (black) and w/o (red) mass uncertainty.

where  $d\mathbf{w}_t \in \mathbb{R}^3$  is a Wiener process and  $\gamma$  is the constant acceleration disturbance intensity.

The continuous-time dynamics are linearized and discretized with  $N = 60$ . The initial nominal trajectory is generated by solving a deterministic minimum-fuel problem using CasADi solver.

The spacecraft is required to move from an initial distribution  $\mathcal{N}(\bar{\mathbf{x}}_i, P_i)$  to a final distribution  $\mathcal{N}(\bar{\mathbf{x}}_f, P_f)$ . The initial state uncertainty is set to  $\sigma_{r_i} = 10$  km and  $\sigma_{v_i} = 0.1$  km/s, with a known initial mass ( $\sigma_{m_i} = 0$ ), resulting in

$$P_i = \text{diag}(10^2, 10^2, 10^2, 10^{-2}, 10^{-2}, 10^{-2}, 0) \quad (\text{km}^2, (\text{km/s})^2, \text{kg}^2). \quad (36)$$

The final state is constrained to  $\sigma_{r_f} = 3.16 \times 10^5$  km and  $\sigma_{v_f} = 0.1$  km/s, with no explicit constraint on the final mass uncertainty, yielding

$$P_f = \text{diag}(10^{11}, 10^{11}, 10^{11}, 10^{-2}, 10^{-2}, 10^{-2}, 5000) \quad (\text{km}^2, (\text{km/s})^2, \text{kg}^2). \quad (37)$$

Please note that a large, unpenalized variance is permitted for the final mass, reflecting that the control objective does not involve regulating the final mass uncertainty. The boundary conditions and physical parameters are summarized in Table II.

TABLE II: Parameters for the 3D Earth-to-Mars problem.

Param.	Value	Unit
$\bar{\mathbf{r}}_i$	$[-140699693; -51614428; 980]$	km
$\bar{\mathbf{v}}_i$	$[9.774596; -28.07828; 4.337725 \times 10^{-4}]$	km/s
$\bar{\mathbf{r}}_f$	$[-172682023; 176959469; 7948912]$	km
$\bar{\mathbf{v}}_f$	$[-16.427384; -14.860506; 9.21486 \times 10^{-2}]$	km/s
$\bar{m}_i$	5000	kg
$\mu$	$1.3271 \times 10^{11}$	$\text{km}^3/\text{s}^2$
$I_{\text{sp}}$	3000	s
$g_0$	$9.80665 \times 10^{-3}$	$\text{km/s}^2$
$u_{\text{max}}$	5	N
$\gamma$	$9 \times 10^{-5}$	$\text{km/s}^{3/2}$
$t_f$	348.795	day

The problem was scaled with a factor of  $d = 100$  for numerical conditioning and solved. The SCP termination criteria were set to  $\varepsilon_x = 5.0 \times 10^{-4}$  and  $\varepsilon_\zeta = 1.0 \times 10^{-6}$ .

The solver converged to a feasible solution in 12 iterations, demonstrating the method's robustness and scalability to a problem with 7 states, 3 control inputs and with  $N = 60$  grid points.

Unlike the position and velocity states, the initial mass is assumed to be known precisely ( $\sigma_{m_i} = 0$ ), reflecting accurate pre-launch propellant loading measurements. However, mass becomes a stochastic variable over time because the control input  $\mathbf{u}_t$ , which has an associated execution uncertainty, directly drives the mass rate equation  $dm_t/dt \propto -\|\mathbf{u}_t\|$ . This propagated mass uncertainty then couples back into the translational dynamics. The state transition matrix (STM) includes the sensitivity of acceleration to mass variations,  $\partial(\mathbf{u}_t/m_t)/\partial m_t = -\mathbf{u}_t/m_t^2$ , creating a feedback loop where uncertainty in mass induces uncertainty in the achieved acceleration for a given thrust command.

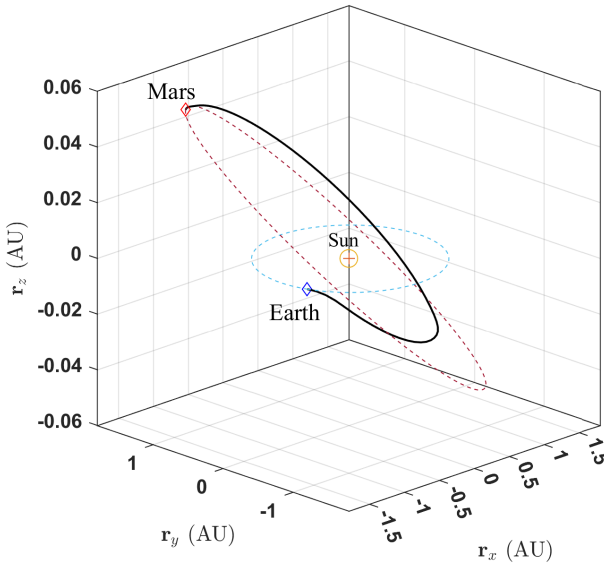
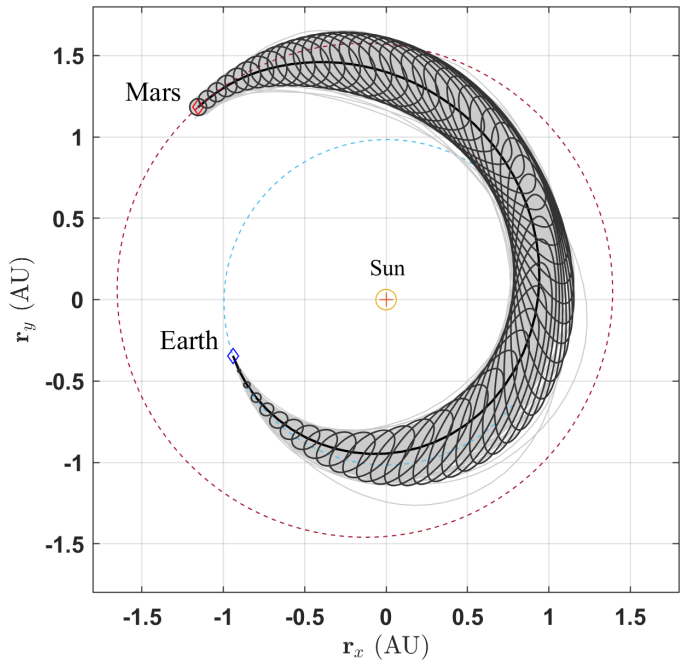
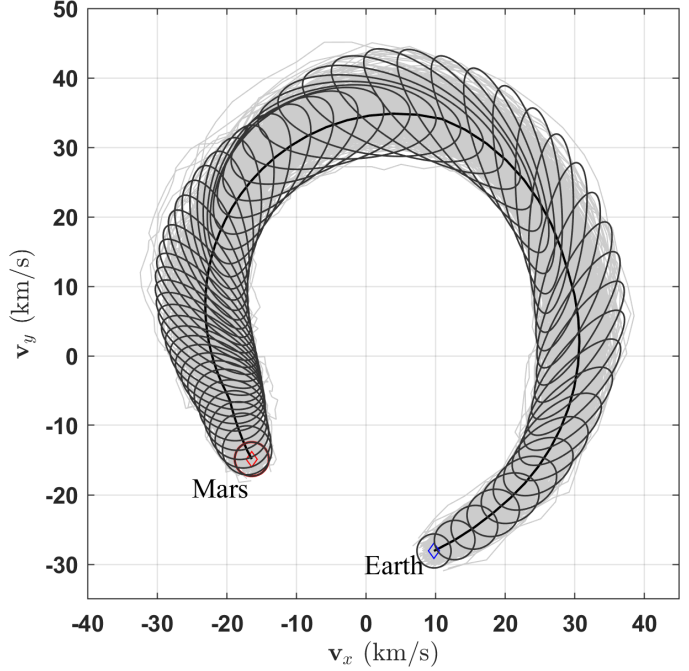


Fig. 8: 3D view of the deterministic, open-loop trajectory for the Earth-to-Mars problem.

The optimized controller successfully navigates the uncertain dynamics to meet the stringent terminal constraints. Figure 8 shows the resulting 3D nominal trajectory, illustrating the spacecraft's path from Earth to Mars in the high-fidelity dynamical model. A Monte Carlo simulation with 1000 samples validates the controller's performance and the accuracy of the covariance propagation. Figure 9 shows the  $x$ - $y$  projection of the closed-loop solution, where the position and velocity covariance ellipses are scaled by a factor of 10 for visual clarity. The close alignment of the Monte Carlo samples with the predicted 95%-confidence ellipses confirms the fidelity of the linearized covariance dynamics within the SCP loop. The control profile, shown in Figure 10, consists of three primary thrust arcs. The nominal thrust magnitude shows a modulated profile, deviating from a pure bang-bang structure to maintain the required robustness margins. The control covariance ellipsoids remain within the thrust upper limit, confirming chance constraint satisfaction.



(a) Closed-loop position covariances (10x).



(b) Closed-loop velocity covariances (10x).

Fig. 9: Monte Carlo validation (1000 samples) within the 95%-confidence ellipses.

One of our main analyses involves a direct comparison between the full stochastic-mass model and a simplified model where mass is treated deterministically. Figure 11 shows the time history of the mass and its standard deviation. The mean mass decreases by approximately 25% over the course of the mission, reaching a final value of approximately  $m_f = 3775$  kg upon arrival at Mars. The mass standard deviation grows from zero to a final value of over 60 kg, driven entirely by the cumulative uncertainty in thrust

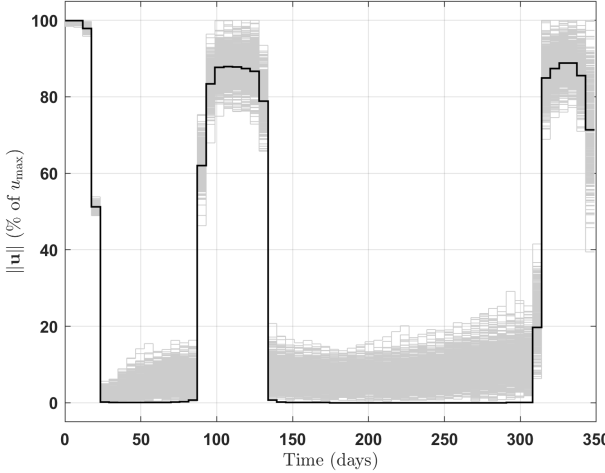


Fig. 10: Control thrust magnitude (top) and components (bottom) with associated  $3\sigma$  uncertainty ellipsoids, demonstrating bounded stochastic control actions.

execution.

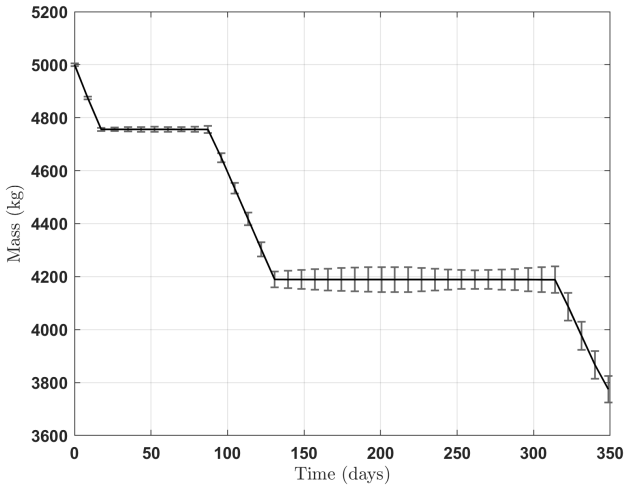


Fig. 11: Time history of spacecraft mass and its standard deviation. The mass uncertainty grows from an initial value of zero due to the stochastic nature of the control inputs.

This mass uncertainty has a notable impact on the translational states. Figure 12 shows the velocity standard deviation along the first principal component. The model with mass uncertainty (black) exhibits a peak velocity dispersion up to 17.73% higher than the deterministic-mass model (red). This inflation occurs because mass uncertainty directly translates into acceleration uncertainty via the  $1/m_t$  term in the dynamics. The effect on the overall position dispersion is summarized in Figure 13, which plots the trace of the position covariance matrix. Inclusion of mass uncertainty results in a 35.21% higher peak position dispersion during the mid-course phase. This notable increase highlights that neglecting mass uncertainty leads to a significant underestimation of the required control authority and the true mission risk.

Finally, Figure 14 compares the nominal control profiles.

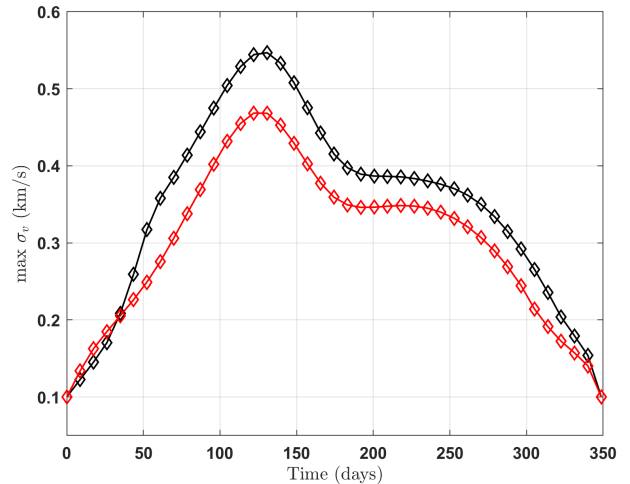


Fig. 12: Velocity standard deviation comparison. The model with mass uncertainty (black) shows significantly higher dispersion, especially during high-thrust phases.

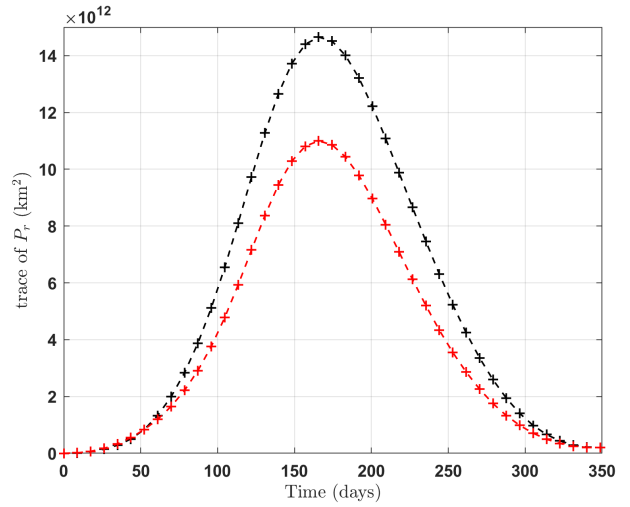


Fig. 13: Trace of position covariance. The formulation with mass uncertainty (black) results in up to 35.21% larger dispersion than the deterministic-mass model (red), highlighting the critical need to model this effect.

The controller for the full stochastic-mass model (black) commands up to 6% higher thrust during the main arcs compared to the deterministic-mass controller (red). This additional control effort is necessary to counteract the larger predicted dispersions and actively shape the covariance, confirming that robustness to mass uncertainty carries a tangible fuel and performance cost.

This 3D case study conclusively demonstrates two key findings. First, the covariance-variable formulation is highly effective for robust trajectory optimization in complex, high-dimensional astrodynamics problems. Second, and more critically, the propagation of mass uncertainty has a substantial, quantifiable impact on both state dispersion and control effort. Neglecting this coupling, as is common in previously simplified models in the literature, leads to an underes-

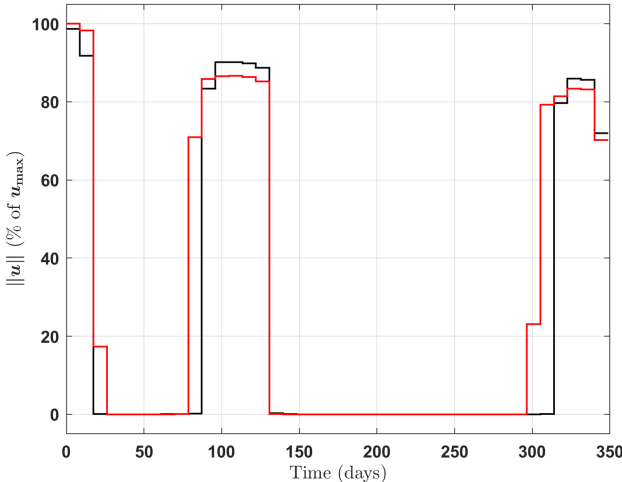


Fig. 14: Comparison of nominal control thrust magnitudes. The controller accounting for mass uncertainty (black) requires higher thrust levels to achieve the same terminal covariance bounds as the controller that neglects it (red).

timation of mission risk and an underpowered controller. The proposed framework successfully manages this coupled uncertainty, providing a robust and high-fidelity solution for generating robust interplanetary guidance algorithms.

## V. CONCLUSIONS

This work presents a sequential convex programming framework for solving the chance-constraint covariance steering problem for low-thrust interplanetary transfers. The method incorporates a piecewise affine state-feedback policy and explicitly models spacecraft mass dynamics within the stochastic formulation. By coupling the control input and disturbance intensity through the time-varying spacecraft mass, the framework captures the evolution of uncertainty more realistically than conventional approaches.

Numerical results successfully demonstrate the regulation of both the mean trajectory and the state covariance, producing closed-loop solutions that satisfy probabilistic terminal constraints and remain consistent with Monte Carlo dispersion analysis. In particular, the inclusion of mass as a stochastic state reveals critical differences in both control effort and uncertainty evolution that are overlooked when mass is treated deterministically. Future studies will apply the computationally efficient proposed method to more challenging trajectory optimization problems [25].

## REFERENCES

- [1] E. Trélat, “Optimal control and applications to aerospace: some results and challenges,” *Journal of Optimization Theory and Applications*, vol. 154, no. 3, pp. 713–758, 2012.
- [2] E. Taheri and J. L. Junkins, “Generic smoothing for optimal bang-off-bang spacecraft maneuvers,” *Journal of Guidance, Control, and Dynamics*, vol. 41, no. 11, pp. 2470–2475, 2018.
- [3] E. Taheri and N. Li, “L2 norm-based control regularization for solving optimal control problems,” *IEEE Access*, vol. 11, pp. 125 959–125 971, 2023.
- [4] R. Bellman, “Dynamic programming,” *Science*, vol. 153, no. 3731, p. 34–37, July 1966.
- [5] J. M. Lee and J. H. Lee, “Approximate dynamic programming strategies and their applicability for process control: A review and future directions,” *International Journal of Control Automation and Systems*, vol. 2, pp. 263–278, 2004.
- [6] D. H. Jacobson and D. Q. Mayne, “Differential dynamic programming,” *American Elsevier Pub. Co.*, 1970.
- [7] N. Ozaki, S. Campagnola, and R. Funase, “Tube stochastic optimal control for nonlinear constrained trajectory optimization problems,” *Journal of Guidance, Control, and Dynamics*, vol. 43, no. 4, p. 645–655, Apr. 2020.
- [8] Y. Chen, T. T. Georgiou, and M. Pavon, “Optimal steering of a linear stochastic system to a final probability distribution, part i,” *IEEE Transactions on Automatic Control*, vol. 61, no. 5, p. 1158–1169, May 2016.
- [9] —, “Optimal steering of a linear stochastic system to a final probability distribution, part ii,” *IEEE Transactions on Automatic Control*, vol. 61, no. 5, p. 1170–1180, May 2016.
- [10] —, “Optimal steering of a linear stochastic system to a final probability distribution—part iii,” *IEEE Transactions on Automatic Control*, vol. 63, no. 9, p. 3112–3118, Sept. 2018.
- [11] T. Lew, R. Bonalli, and M. Pavone, “Chance-constrained sequential convex programming for robust trajectory optimization,” in *2020 European Control Conference (ECC)*. IEEE, May 2020, p. 1871–1878.
- [12] J. Ridderhof, K. Okamoto, and P. Tsiotras, “Nonlinear uncertainty control with iterative covariance steering,” in *2019 IEEE 58th Conference on Decision and Control (CDC)*, 2019, pp. 3484–3490.
- [13] J. Ridderhof, J. Pilipovsky, and P. Tsiotras, “Chance-constrained covariance control for low-thrust minimum-fuel trajectory optimization,” in *AAS/AIAA Astrodynamics Specialist Conference*, 2020, pp. 9–13.
- [14] V. Renganathan, J. Pilipovsky, and P. Tsiotras, “Distributionally robust covariance steering with optimal risk allocation,” 2022. [Online]. Available: <https://arxiv.org/abs/2210.00050>
- [15] B. Benedikter, A. Zavoli, Z. Wang, S. Pizzurro, and E. Cavallini, “Convex approach to covariance control with application to stochastic low-thrust trajectory optimization,” *Journal of Guidance, Control, and Dynamics*, vol. 45, no. 11, p. 2061–2075, Nov. 2022.
- [16] G. Rapakoulias and P. Tsiotras, “Comment on “convex approach to covariance control with application to stochastic low-thrust trajectory optimization”,” *Journal of Guidance, Control, and Dynamics*, vol. 46, no. 5, p. 1023–1024, May 2023.
- [17] N. Kumagai and K. Oguri, “Robust cislunar low-thrust trajectory optimization under uncertainties via sequential covariance steering,” *Journal of Guidance, Control, and Dynamics*, p. 1–19, Aug. 2025.
- [18] F. Liu, G. Rapakoulias, and P. Tsiotras, “Optimal covariance steering for discrete-time linear stochastic systems,” *IEEE Transactions on Automatic Control*, 2024.
- [19] J. Ridderhof and P. Tsiotras, “Minimum-fuel closed-loop powered descent guidance with stochastically derived throttle margins,” *Journal of Guidance, Control, and Dynamics*, vol. 44, no. 3, pp. 537–547, 2021.
- [20] Y. Zhang, M. Cheng, B. Nan, and S. Li, “Stochastic trajectory optimization for 6-dof spacecraft autonomous rendezvous and docking with nonlinear chance constraints,” *Acta Astronautica*, vol. 208, pp. 62–73, 2023.
- [21] J. Pilipovsky and P. Tsiotras, “Computationally efficient chance constrained covariance control with output feedback,” in *2024 IEEE 63rd Conference on Decision and Control (CDC)*. IEEE, Dec. 2024, p. 677–682.
- [22] E. Taheri, I. Kolmanovsky, and E. Atkins, “Enhanced smoothing technique for indirect optimization of minimum-fuel low-thrust trajectories,” *Journal of Guidance, Control, and Dynamics*, vol. 39, no. 11, pp. 2500–2511, 2016.
- [23] N. P. Nurre and E. Taheri, “Comparison of indirect and direct methods for operationally constrained low-thrust trajectories,” *Journal of Guidance, Control, and Dynamics*, vol. 48, no. 4, pp. 885–902, 2025.
- [24] J. A. Andersson, J. Gillis, G. Horn, J. B. Rawlings, and M. Diehl, “Casadi: a software framework for nonlinear optimization and optimal control,” *Mathematical Programming Computation*, vol. 11, no. 1, pp. 1–36, 2019.
- [25] N. P. Nurre and E. Taheri, “Constrained fuel-and time-optimal six-degree-of-freedom powered descent guidance using indirect optimization,” *Journal of Spacecraft and Rockets*, pp. 1–22, 2025.